Global and Planetary Change 220 (2023) 103997

Contents lists available at ScienceDirect

Global and Planetary Change

journal homepage: www.elsevier.com/locate/gloplacha

Opposite mass balance variations between glaciers in western Tibet and the western Tien Shan

Meilin Zhu [a,c,*], Lonnie G. Thompson [c], Tandong Yao [b], Shengqiang Jin [b], Wei Yang [b], Yang Xiang [d], Huabiao Zhao [b,e,**]

[a] Center for the Pan-Third Pole Environment, Lanzhou University, Lanzhou 730000, China
[b] State Key Laboratory of Tibetan Plateau Earth System, Resources and Environment, Institute of Tibetan Plateau Research, Chinese Academy of Sciences (CAS), Beijing 100101, China
[c] Byrd Polar and Climate Research Center, The Ohio State University, Columbus, OH 43210, USA
[d] College of Geomatics, Xi'an University of Science and Technology, Xi'an 710054, Shaanxi, China
[e] Ngari Station for Desert Environment Observation and Research, Institute of Tibetan Plateau Research, CAS, Tibet, China

ARTICLE INFO

Editor: Jed O Kaplan

Keywords:
Glacier mass balance
Western Tibet
Western Tien Shan
Atmospheric circulation
Sea surface temperature

ABSTRACT

Understanding the spatiotemporal variability of glacier mass balance in the Third Pole (TP) is important in the predictability of regional water supplies and glacier-related natural hazards. However, it is unclear how interannual mass balance variations in glaciers located within different climatic regions of the TP relate to each other. This study studied ablation season (June-September) mass balance variations between glaciers situated in western Tibet, which lies on the transition between monsoon-dominated and westerlies-dominated regions, and the western Tien Shan, which is a region dominated by westerlies. We investigated how these glacier mass balance variations correlated with major atmospheric circulation patterns from 1970 to 2019. At interannual timescales, we showed that ablation season mass balance variations were related to ablation season air temperature and ablation season precipitation in the western Tien Shan, whereas variations in western Tibet were mainly controlled by ablation season precipitation. Further analysis identified a seesaw-style phenomenon in ablation season mass balance variations between the western Tien Shan and western Tibet. These spatial variations resulted from opposing responses of mass balance to shifts in the subtropical westerly jet position during the ablation season. When the subtropical westerly jet moves southward, the western Tien Shan receives a larger amount of precipitation and colder air temperature, which contributes to less negative ablation season mass balance. Concurrently, western Tibet receives less ablation season precipitation, which reduces ablation season mass balance. When the subtropical westerly jet moves northward, these responses are reversed. Changes in the subtropical westerly jet position are influenced by atmospheric circulation in Europe through the European–Asian teleconnection, and by sea surface temperature in the northern Arabian Sea through the Central-Asia–tropical-Indian-Ocean teleconnection. This indicates that interactions between the South Asian monsoon and the westerlies cause opposite ablation season mass balance variations between glaciers in western Tibet and the western Tien Shan at interannual timescales.

1. Introduction

The Tibetan Plateau, Himalayas, Hindu Kush, Pamirs, and Tien Shan Mountains are collectively known as the Earth's Third Pole (TP) (Yao et al., 2019), which contains the largest number of glaciers outside of the polar regions (Yao et al., 2012). These glaciers provide an important supply of fresh water to major Asian rivers (Aizen et al., 1997; Barandun et al., 2021; Immerzeel et al., 2019; Pritchard, 2019; Sorg et al., 2012), which delivers water to almost two billion people (Yao et al., 2022). Glacier mass balance variations can be used to link glacier change with hydrological processes and have been studied in different regions of the TP using in-situ measurements, remote sensing data and modelling

* Corresponding author at: Center for the Pan-Third Pole Environment, Lanzhou University, Lanzhou 730000, China.
** Corresponding author at: Key Laboratory of Tibetan Environment Changes and Land Surface Processes, Institute of Tibetan Plateau Research, Chinese Academy of Sciences (CAS), Beijing 100101, China.
E-mail addresses: zhuml@lzu.edu.cn (M. Zhu), zhaohb@itpcas.ac.cn (H. Zhao).

https://doi.org/10.1016/j.gloplacha.2022.103997
Received 19 June 2022; Received in revised form 31 October 2022; Accepted 24 November 2022
Available online 30 November 2022
0921-8181/

(Azam and Srivastava, 2020; Brun et al., 2017; Barandun et al., 2015, 2018; Bhattacharya et al., 2021; Farinotti et al., 2015; Fujita and Ageta, 2000; Fujita et al., 2011; Fujita and Nuimura, 2011; Hugonnet et al., 2021; Kenzhebaev et al., 2017; Kronenberg et al., 2021; Van Tricht et al., 2021; Wang et al., 2020; Yang et al., 2016; Yao et al., 2019; Zemp et al., 2019; Zhang et al., 2020; Zhou et al., 2018; Zhu et al., 2018, 2021a, 2022a).

Direct in-situ measurements of mass balance have been conducted on several glaciers in the TP since the 1950s, including those in the Tien Shan, Pamir-Alay, Qilian Mountains, and Himalayas (Dyurgerov, 2002; Shi et al., 2000; WGMS, 2021; Yao et al., 2012; Zhang et al., 2021). Most glacier-monitoring operations in the Tien Shan and Pamir-Alay were interrupted after collapse of the Union of Soviet Socialist Republics (USSR) in the early 1990s (Hoelzle et al., 2017). In addition, the most monitored glaciers on the Tibetan Plateau have been observed for a few years, and the monitoring operations were largely discontinuous between the 1950s and 1990s (Shi et al., 2000). Continuous monitoring activities during this period were maintained for a few glaciers, such as Ts. Tuyuksu Glacier (WGMS, 2021), Urumqi Glacier No. 1 (Wang et al., 2020; WGMS, 2021), and Xiao Dongkemadi Glacier (Pu et al., 2008). Reestablished and newly established monitoring operations have been undertaken on several glaciers in different climatic regions of the TP since 2000, such that the number of monitored glaciers continues to increase (Hoelzle et al., 2017; WGMS, 2021; Yao et al., 2012, 2022). In recent decades, remote sensing data obtained through sources including the Gravity Recovery and Climate Experiment, digital elevation models using optical images and radar data, and the Ice, Cloud, and Land Elevation Satellite (ICESat) have been used to obtain regionally averaged mass balance variations for various glaciers in the TP over multiyear or decadal timescales (Bhattacharya et al., 2021; Brun et al., 2017; Hugonnet et al., 2021; Yao et al., 2022). Nonetheless, there are still difficulties associated with obtaining the continuous mass balance time series for individual glaciers at annual and seasonal timescales (Barandun et al., 2020).

Glacier models have been used to derive continuous mass balance time series for selected glaciers in the TP (e.g. Barandun et al., 2015; Kronenberg et al., 2016; Liu and Liu, 2016; Kenzhebaev et al., 2017; Farinotti et al., 2015; Zhu et al., 2018, 2021b). However, the modelled results depend strongly on model's calibration and the quality of the input variables (Barandun et al., 2018; Zhu et al., 2021b). For example, choosing appropriate climate variables time series strongly influences whether or not modelled mass balance time series closely matches measured data (Zhu et al., 2020, 2021b).

These past research projects have demonstrated an accelerated loss of mass from most glaciers in the TP in recent decades, except for those in the eastern Pamir, Karakoram, and western Kunlun regions. Indeed, these glaciers remained stable or even expanded in size and volume. When combined with regional climate change, these glacier variations have caused glacier-related disasters to become more unpredictable and have increased the future vulnerability of water resources in those river basins (Bazai et al., 2020; Cook et al., 2018; Immerzeel et al., 2019; Huss and Hock, 2018; Marzeion et al., 2014; Radić and Hock, 2011; Thompson et al., 2021). Hence, it is necessary to understand the spatiotemporal variability of glacier mass balance in the TP and associated drivers. Recent studies have focused mainly on single glaciers or several glaciers within the monsoon or westerlies region (Azisov et al., 2022; Barandun et al., 2018, 2021; Kenzhebaev et al., 2017; Kronenberg et al., 2021; Mölg et al., 2014; Van Tricht et al., 2021; Yang et al., 2016; Zhu et al., 2021a, 2022b). These studies showed that TP glaciers could experience different changes due to different climate changes at interannual timescales. Comparison of glacier mass balance variations between different climate regions can improve our understanding of the coordinated variation of glacier mass balance and associated atmospheric circulation across the larger TP region. However, analyses that compare interannual variations in glacier mass balance across different climatic regions in the TP have not been carried out.

The TP can be divided into three climate regions: the monsoon-dominated region (south of 31°N to 32°N), the westerlies-dominated region (north of 34°N to 35°N), and the transitional area between the two (Fig. 1, Thompson et al., 2018, Yao et al., 2013). The western Tien Shan and western Tibet are located in the westerlies-dominated region and transition region, respectively. The subtropical westerly jet position impacts the climate in both regions (Aizen et al., 1997, 2001; Mölg et al., 2017; Zhu et al., 2021b). For example, the southward shift of the subtropical westerly jet is accompanied by increased summer rainfall over the domain 55-85°E and 35-50°N (which includes the western Tien Shan region, Zhao et al., 2018), but reduced summer precipitation in western Tibet (Mölg et al., 2017; Zhu et al., 2021b). Glacier mass balance variations are driven mainly by climatic factors (Oerlemans, 2005; Zhu et al., 2020, 2021b). Thus, it is possible that there are correlation relationships in terms of glacier mass balance between the two regions. Some researchers have analyzed glacier mass balance variations in the western Tien Shan and western Tibet, which provided measured or reconstructed long-term seasonal mass balance data (Azisov et al., 2022; Barandun et al., 2015, 2018; Dyurgerov, 2002; Hoelzle et al., 2017; Kenzhebaev et al., 2017; Kronenberg et al., 2021; Van Tricht et al., 2021; WGMS, 2021; Zhu et al., 2021b). These studies provided an opportunity to quantify glacier mass balance variations at interannual timescales for these two regions. The aims of this study are as follows: (1) to quantitatively investigate the differences in interannual variations in glacier mass balance from 1970 to 2019, between the western Tien Shan and western Tibet; and (2) to identify the drivers and establish the relationships between mass balance variations and atmospheric circulation systems between these two regions.

2. Study area, data, and methods

2.1. Study area and glacier mass balance data

Xiao Anglong Glacier is a valley-type glacier in western Tibet (Fig. 1), situated within the area of transition between the westerlies-dominated and monsoon-dominated climate regimes. Its area and altitude distribution are listed in Table 1. An automatic weather station (AWS) was established at 5141 m a.s.l. (32°54′38.14"N, 80°50′13.58″E) in August 2014, approximately 7.5 km northeast of Xiao Anglong Glacier. Meteorological records at this AWS from October 1st, 2014 to September 30th, 2019, showed a mean annual precipitation of 224 mm, with 86.3% of this total occurring in the ablation season, and maximum monthly precipitation rates documented in July and August (Zhu et al., 2021b). Zhu et al. (2021b) reconstructed the seasonal mass balance for Xiao Anglong Glacier from 1968 to 2019. Annual mass balance series have similar variation patterns when they are located in a region with similar climate changes (Liu and Liu, 2016; Mölg et al., 2014; Zhu et al., 2018). Thus, variations in mass balance on Xiao Anglong Glacier can be used to represent those on regional glaciers in western Tibet.

Glaciers in the western Tien Shan and Pamir-Alay are controlled mainly by westerlies (Fig. 1 and Fig. S1 in the supplementary material, Chen et al., 2019; Yao et al., 2013). Considering the significant and positive relationships of annual mass balance between Abramov Glacier in the Pamir-Alay and some glaciers (such as Ts. Tuyuksu and Kara-Batkak glaciers) in the western Tien Shan (Fig. 1 and Fig. S1, Liu and Liu, 2016), the Tien Shan and Pamir-Alay can be roughly divided into western Tien Shan and eastern Tien Shan. Here we focused on glacier mass balance variations in the selected region of the western Tien Shan (39.25–43.25°N, 71.25–79.25°E) which contains Ts. Tuyuksu, Kara-Batkak, and Abramov glaciers (Fig. 1). Direct mass balance measurements have been conducted on several glaciers in the western Tien Shan since the 1950s, and some glacier-monitoring operations were interrupted between the 1990s and 2010s (Dikikh, 1982; Dyurgerov et al., 1995; Dyurgerov, 2002; Glazyrin, 1985; Hoelzle et al., 2017; Makarevich, 1984; Makarevich et al., 1985; Satylkanov, 2018; WGMS, 2021). Among these, Ts. Tuyuksu, Kara-Batkak, Abramov, Sary Tor, Batysh

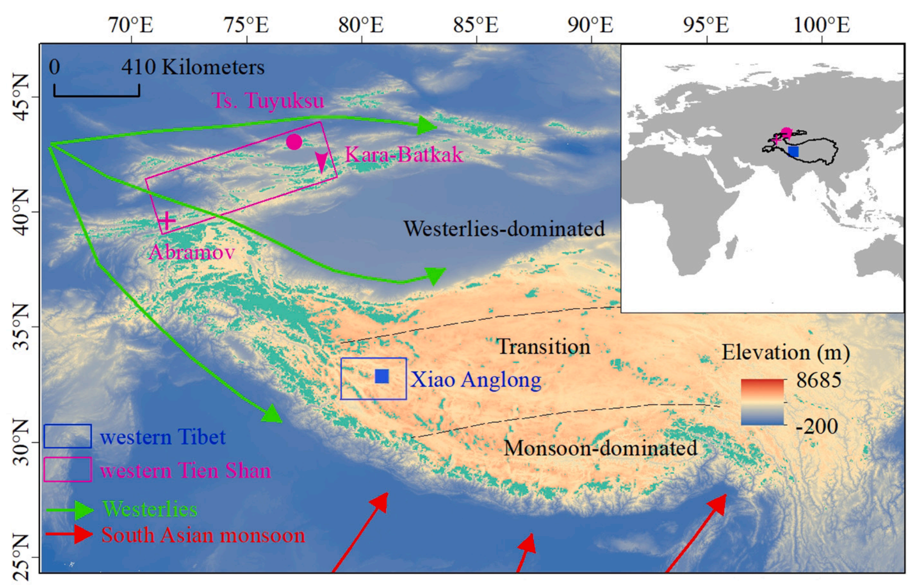

Fig. 1. Geographical locations of the study area and selected glaciers. Arrows indicate the major atmospheric circulation systems around the Tibetan Plateau. Blue and pink polygons indicate the selected regions of western Tibet and the western Tien Shan, respectively. Symbols are as follows: pink dot, Ts. Tuyuksu Glacier; pink inverted triangle, Kara-Batkak Glacier; pink cross, Abramov Glacier; blue square, Xiao Anglong Glacier. Black dashed lines separate the TP into three major climate regimes: monsoon-dominated region, westerlies-dominated region, and their transitional region (and Thompson et al., 2018; Yao et al., 2013). Glaciers are marked by a jade colour. Inset box shows the global location of the selected glaciers. (For interpretation of the references to colour in this figure legend, the reader is referred to the web version of this article.)

Table 1
List of studied glaciers in this study.

	Name	Latitude (°)	Longitude (°)	Altitude extent (Min–Max, m a.s.l.)	Area (km^2)	Periods used in this study	Origin
Western Tien Shan	Ts. Tuyuksu	43.05	77.08	3500-4220	2.8	1970-2019[a]	In-situ measurements from WGMS, (2021)
	Kara-Batkak	42.14	78.27	3275-4829	2.5	1976-1990[a], 1996-998[a] and 2014-2019[a]	
	Sary Tor	41.83	78.174	3950-4800	2.6	1985-1989[a] and 2015-2019[a]	
	Abramov	39.62	71.56	3619-5000	24.9	1971-1994[a] and 2012-2019[a]	
	Batysh Sook	41.79	77.75	3944-44,471	1.1	1971[a], 1984[a], 1989[a] and 2011-2019[a]	
	Glacier No. 354 (Akshiyrak)	41.799	78.151	3746-4700	6.4	2011-2019[a]	
	Golubin	42.46	74.495	3225-4437	5.9	1970-1994[a] and 2011-2019[a]	
Western Tibet	Xiao Anglong	32.85	80.901	5769-6467	1.55	1970-2019[b]	Reconstructed values from Zhu et al., (2021b)

[a] In-situ measurements of mass balance used in this work.
[b] Reconstructed mass balance used in this work. Ablation season mass balance of Abramov Glacier in 1984 is the modelled value from Barandun et al. (2015).

Sook, No. 354 (Akshiyrak), and Golubin glaciers were measured at seasonal time scales (Table 1). Measurements of Tuyuksu, Kara-Batkak, and Abramov glaciers included ablation season and cold season (October-May) mass balance data that span more than 20 years, although in-situ measurements of mass balance on Kara-Batkak and Abramov glaciers were not taken consecutively. Ablation stakes installed on the glaciers and snow-pit features (snow layer density and stratigraphy) were measured at the end of the accumulation season (typically at the end of May) and at the end of the ablation season (September) (Dyurgerov, 2002; WGMS, 2021). Thus, these three glaciers were selected as being representative glaciers in the selected region of the western Tien Shan (Fig. 1), and their measured seasonal mass balances were used here, since annual mass balance time series have similar variation patterns (Liu and Liu, 2016). For Ts. Tuyuksu Glacier, precipitation mainly occurred in spring and summer, and precipitation was higher in the former than the latter, with maximum precipitation occurring in late spring. For Abramov Glacier, most precipitation occurred in winter, and spring, with maximum precipitation in early spring. For Kara-Batkak Glacier, precipitation mainly occurred in spring and summer, with maximum precipitation in late spring and early summer (Liu and Liu, 2016; Kronenberg et al., 2016; Shahgedanova et al., 2018; Van Tricht et al., 2021; Fig. S2 in the supplementary material). Above all, those four glaciers showed notable seasonal variations in precipitation, with a higher ratio of cold season precipitation to annual precipitation occurring noted for Ts. Tuyuksu and Abramov glaciers relative to that for Kara-Batkak and Xiao Anglong glaciers, while air temperature (T_a) was higher during summer than in other seasons (Fig. S2 in the supplementary material).

2.2. Meteorological data and index definitions

The following data products were used to investigate variations in glacier mass balance at the regional scale: (1) monthly air temperature and total precipitation data obtained from the Climatic Research Unit dataset (CRU TS v. 4.04, 0.5° × 0.5°, for 1901–2019) (Harris et al., 2020); (2) monthly sea surface temperatures (SST) obtained from the Hadley Centre Sea Ice and Sea Surface Temperature dataset (HadISST, 1° × 1°, Rayner et al., 2003); and (3) monthly geopotential height and wind fields at 600 hPa and 300 hPa obtained from the Japanese 55-year reanalysis dataset (JRA55, 1.25° × 1.25°, 1958–2019, Kobayashi et al., 2015). Monthly precipitation and air temperature data from the CRU represent the gridded interpolation of existing instrumental data from meteorological stations. The CRU dataset produced before the 1960s is not suitable for some applications because of its limited gauge number, thus, we used the latest 50-year data from 1970 to 2019 in this study. Previous studies have shown that CRU data strongly correlates with local data from the Tibetan Plateau and Central Asia, and the CRU data accurately capture the main features of interannual variations in air temperature and precipitation (Hu et al., 2014; Mannig et al., 2013; Shi et al., 2017; Wang et al., 2013; Yao et al., 2020; Zhao and Fu, 2006). In addition, considering that sparse observational climate data exist within the TP, monthly CRU gridded data are often used as a reference dataset with which to study climate change, glacier change, and lake change (Shi et al., 2015; Wang et al., 2019; Zhang et al., 2020; Zhu et al., 2021a). Thus, the CRU dataset is known to have an acceptable level of precision and is considered as a reliable climatic data source for the TP. Additionally, SST value from the HadISST and climate parameters from JRA55 datasets have been used extensively in climate change research, and represent an important data source for many researchers around the world (Chen et al., 2020; Gao et al., 2016; Harada et al., 2016).

The Silk Road Pattern (SRP) is a zonally oriented teleconnection pattern that occurs over Eurasia during the boreal summer. It propagates along the upper-tropospheric Asian westerly jet and has several geographically fixed centers (Enomoto et al., 2003; Lu et al., 2002). With a broad extent from Europe to East Asia, the SRP exerts a strong influence on climate (i.e. precipitation and air temperature) patterns in these regions (Enomoto et al., 2003; Hong et al., 2018). Following Yasui and Watanabe (2010), SRP data were obtained by applying empirical orthogonal function (EOF) analysis to JRA55 raw ablation season 200-hPa meridional wind (V200) anomalies within the spatial domain 20°–60°N and 0°–150°E, after which the leading mode was determined (Hong et al., 2018). The standardized principal component of this leading mode (PC1) was then taken as the SRP index (SRPI) in order to quantify the SRP. This mode accounts for 28.9% of the total variance for the V200 anomalies and can be easily discriminated from the second mode, which accounts for 9.9% of the total variance. The global wave train index (GTI, Fig. S3) was used to indicate the state of the westerlies, and was determined as the anomaly with respect to the 200 hPa geopotential height averaged over the spatial domain 35–40°N and 60–70°E (Ding and Wang, 2005). The subtropical westerly jet position index (SWJPI) is defined as the average zonal wind at 200 hPa in a southern region (30–45°N, 50–80°E) minus the one in a northern region (45–60°N, 50–80°E) (Zhao et al., 2014), which was calculated based on JRA55 data. Positive deviations in the normalized time series of such an index indicate a more southerly jet position (Mölg et al., 2017; Zhao et al., 2014).

2.3. Methods

Interannual variability and linear trend of data affect correlations between data from multiple time series. When a linear trend is removed from a time series, a correlation coefficient can be used to highlight the relationships between these data at interannual timescales. Thus, to understand how climate influences interannual variations in glacier mass balance, it is necessary to remove linear trends from the time series data. Hence, the detrended time series data ($y_{detrend\_i}$) were calculated using the following equation:

$$y_{slope} = \frac{\sum_{i=1}^{n}(x_i - \overline{x})(y_i - \overline{y})}{\sum_{i=1}^{n}(x_i - \overline{x})^2} \tag{A1}$$

$$y_{intercept} = \overline{y} - y_{slope} \times \overline{x} \tag{A2}$$

$$y_{trend\_i} = x_i \times y_{slope} + y_{intercept} \tag{A3}$$

$$y_{detrend\_i} = y_i - y_{trend\_i} \tag{A4}$$

where x_i and y_i are the i^{th} independent and dependent variables, respectively; $\overline{x}$ and $\overline{y}$ are the means of the independent and dependent variables, respectively; n is the length of the time series; y_{slope} and $y_{intercept}$ are the slope and intercept of the dependent variables, respectively; and y_{slope} is the trend of dependent variables.

Correlation analysis is a statistical method used to measure the strength of the linear relationship between variables in two separate time series. The correlation coefficient (r) quantifies the strength of the correlation relationship between variables in the both time series, and has a value between 1 and − 1. Here, r was calculated as:

$$r = \frac{\sum_{i=1}^{n}(xa_i - \overline{xa}) \times (ya_i - \overline{ya})}{\sqrt{\sum_{i=1}^{n}(xa_i - \overline{xa})^2} \times \sqrt{\sum_{i=1}^{n}(ya_i - \overline{ya})^2}} \tag{A5}$$

where xa_i and ya_i are variables of each time series; $\overline{xa}$ and $\overline{ya}$ are the means of each set of two time series variables; and n is the length of the time series.

To limit the influence of local climate on regional glacier mass balance variations, a three-year running mean was used for detrended ablation season mass balances of Xiao Anglong and Ts. Tuyuksu glaciers during 1970–2019. The significance of the correlation coefficient was estimated based on Monte Carlo analysis (Di Lorenzo et al., 2010), which was calculated by following a similar method to that documented by Chen et al. (2020). Firstly, two random sequences with the same length (i.e. $n = 50$ in this study) were generated and their correlation coefficient was computed after a three-point running mean. Secondly, the above-described process was repeated 5000 times, the results ranked, and the result with the highest numerical ranking of R0 at M0 (i.e. 5000 × 0.05, at the 0.05 confidence levels) is picked out from the sorted list of 5000 correlation coefficients. Thirdly, the above two processes were repeated 40 times and the average value of all 40 R0s was used as the critical value for correlation coefficients at the 1 − M0/5000 confidence level. In this work, 0.34 (−0.34) was used as the critical value for the correlation coefficient at the 0.05 confidence levels.

3. Results

3.1. Glacier mass balance characteristics in the western Tien Shan

We examined the relationships between mass balances among glaciers in the western Tien Shan at interannual timescales (Table 2) using correlation analysis of seasonal mass balance variations during 1970–2019. The mass balance series of Xiao Anglong Glacier used here considered the reconstructed values due to the lack of long-term in-situ measurements (Zhu et al., 2021b). And the fluctuations in mass balance series between modelled and measured values were similar for Xiao Anglong Glacier (Fig. 3e in Zhu et al., 2021b). Mass balance series for Ts. Tuyuksu, Kara-Batkak, and Abramov glaciers used in this work were formulated from in-situ measurements, although there were some gaps in the dataset for Kara-Batkak and Abramov glaciers.

Table 2 shows that some glaciers in the western Tien Shan (i.e. the Sary Tor, Batysh Sook, and Akshiyrak glaciers) did not show significant correlations with other glaciers, and it is notable that the mass-balance time series for these glaciers have continuous lengths less than 10 years. In addition, although Sary-Tor Glacier and Glacier No. 354 are located only 5 km apart, and the correlation of ablation season mass balance between both glaciers is significant, the correlation of annual mass balance between both glaciers is low, which we interpret to be due to the negative correlation of cold season mass balance between them. Snowdrift may have caused different degrees of cold season snowfall accumulation on both glaciers, given their different morphological characteristics and surface wind speeds. And the uncertainties related to the measured cold season mass balance may also have contributed to the negative correlation of cold season mass balance values between both

Table 2
Correlation coefficients of seasonal mass balances among different glaciers during 1970-2019.

Annual	Ts. Tuyuksu	Kara-Batkak	Sary Tor	Abramov	Batysh Sook	Glacier No. 354 (Akshiyrak)	Golubin
Ts. Tuyuksu	1						
Kara-Batkak	0.59*	1					
Sary Tor	0.22	0.22	1				
Abramov	0.61*	0.34	0.08	1			
Batysh Sook	0.42*	0.72*	0.53	0.17	1		
Glacier No. 354 (Akshiyrak)	0.57	0.33	0.2	0.1	0.76*	1	
Golubin	0.61*	0.3	0	0.26	0.16	0.55	1
Ablation season							
Ts. Tuyuksu	1						
Kara-Batkak	0.54*	1					
Sary Tor	0.1	0.44	1				
Abramov	0.43*	0.4*	0.53	1			
Batysh Sook	0.14	0.24	−0.1	0.48	1		
Glacier No. 354 (Akshiyrak)	0.7*	0.79*	0.68*	0.15	0.53	1	
Golubin	0.55*	0.5*	0.8*	0.58*	0.08	0.81*	1
Cold season							
Ts. Tuyuksu	1						
Kara-Batkak	0.56*	1					
Sary Tor	0.46	−0.22	1				
Abramov	0.16	0.17	−0.1	1			
Batysh Sook	0.02	0.58	−0.09	0.05	1		
Glacier No. 354 (Akshiyrak)	0.52	0.22	−0.42	0.08	−0.42	1	
Golubin	0.15	0.37	−0.5	0.39	0	0.68*	1

* Means that p is less than 0.05.

glaciers.

Glaciers with long-duration time series show similar variations in annual mass balance at interannual timescales, including Ts. Tuyuksu, Kara-Batkak and Abramov glaciers (Table 2). Liu and Liu (2016) also reported that annual mass balance records spanning more than 20 years showed significant positive correlations from 1969 to 1990. In addition, correlation coefficients of ablation season mass balances for Ts. Tuyuksu, Kara-Batkak, and Abramov glaciers from 1970 to 2019 are significant; however, only mass balance measurements for Ts. Tuyuksu and Kara-Batkak glaciers showed significant correlations during cold seasons. There were no significant correlations for mass-balance measurements during the cold season between Abramov and Ts. Tuyuksu glaciers. Such phenomenon may be caused by different interannual variations in local cold season precipitation rates and snowdrift. These correlations indicate that similar variations in annual mass balance for different glaciers in the western Tien Shan were caused primarily by similar mass balance variations during ablation seasons at interannual timescales.

We identified no stable relationships between cold season and ablation season mass balances for individual glaciers in the western Tien Shan from 1970 to 2019. The calculated correlation coefficients between cold season and ablation season mass balances for Ts. Tuyuksu, Kara-Batkak, and Abramov glaciers for that period were − 0.03 ($p > 0.05$, $n = 50$), 0.35 ($p > 0.05$, $n = 24$), and − 0.31 ($p > 0.05$, $n = 32$), respectively. Thus, cold season mass balances have little impact on variations in ablation season mass balance in the western Tien Shan.

Some glaciers in the selected region of the western Tien Shan show mass balance time series with significant mutual positive correlations. Thus, the selected region is not defined by similar climatic regimes in this region, but by similar glacier mass balance variations in this region. Although precipitation seasonalities were slightly different among Ts. Tuyuksu, Kara-Batkak, and Abramov glaciers, interannual variation in ablation season air temperature and precipitation data were similar. The correlation coefficients of detrended ablation season air temperature data between Ts. Tuyuksu and Abramov glaciers, between Ts. Tuyuksu and Kara-Batkak glaciers, and between Kara-Batkak and Abramov glaciers were 0.77 ($p < 0.05$), 0.82 ($p < 0.05$), and 0.88 ($p < 0.05$), respectively. Similarly, correlation coefficients for detrended ablation-season precipitation for the same pairs of glaciers were 0.59 ($p < 0.05$), 0.86 ($p < 0.05$), and 0.61 ($p < 0.05$), respectively. In addition, Fig. 3 and Figs. S4-S5 show that ablation season mass balances of these three glaciers correlated well with ablation season air temperature and ablation season precipitation in the western Tien Shan at interannual timescales. This indicates that variations in air temperature and precipitation during ablation seasons are similar at different sites within the selected region of the western Tien Shan, which supports allocating these three glaciers to the selected region of the western Tien Shan.

3.2. Comparison of ablation season mass balances between glaciers in western Tibet and the western Tien Shan at interannual timescales

According to the mass balance measurements made during 1970-2019 by the WGMS (2021), typical glaciers in the western Tien Shan show positive cold season mass balance values for the most years. Mean cold season mass balance ranged from 332 mm w.e. a^{-1} in Batysh Sook Glacier to 1353 mm w.e. a^{-1} in Abramov Glacier (Table 3). For these glaciers, ablation season mass balances were negative in most years, and mean ablation season mass losses were relatively high, with values ranging from −1779 mm w.e. a^{-1} in Abramov Glacier to −989 mm w.e. a^{-1} in Batysh Sook Glacier (Table 3). Xiao Anglong Glacier, recorded a minor net loss of mass, despite mean mass balance in both the cold and ablation seasons being close to balanced conditions during 1970-2019 (Table 3). Cold season mass balances of Xiao Anglong Glacier were larger than −80 mm w.e. in most years during the period 1970-2019. During ablation seasons, mass balances were mostly positive throughout 1968-1990, and had a mean value of 124 mm w.e. a^{-1}; most mass balances were negative during the period 1991-2012, and had a mean value of −165 mm w.e. a^{-1}; and mass balance became positive again in some years during 2013-2019, with a mean value of 66 mm w.e. a^{-1} (Zhu et al., 2021b). In addition, the absolute values for average cold season mass balance during 1970-2019 for those three glaciers in the Tien Shan were significantly higher than that for Xiao Anglong Glacier in western Tibet due to different seasonal precipitation patterns in both regions (Table 3). These data suggest that Xiao Anglong Glacier is more stable than monitored glaciers in the western Tien Shan.

In addition, for the same glacier in the selected region of the western Tien Shan, ablation season mass balance plays a more important role in controlling variations in annual mass balance than it does for cold season mass balance. This is demonstrated firstly by the higher correlation coefficient between ablation season and annual mass balances relative to that between cold season and annual mass balances (Table 3), and secondly by higher standard deviation for ablation season mass balance

Table 3
The mean values (mm w.e. a^{-1}) and standard deviations (mm w.e) of seasonal mass balance for selected glaciers and the correlation coefficients (r) of seasonal mass balance and annual mass balance for those glaciers during 1970-2019.

Name	Years	Cold season			Ablation season		
		Mean mass balance	r	Standard deviation	Mean mass balance	r	Standard deviation
Western Tien Shan							
Ts. Tuyuksu	50	651	0.45	266	−1142	0.88	422
Kara-Batkak	25	511	0.75	169	−1243	0.88	232
Sary Tor (No.356)	10	411	0.88	123	−927	0.99	386
Abramov	32	1353	0.4	342	−1779	0.74	469
Batysh Sook	13	332	−0.45	229	−989	0.83	584
Western Tibet							
Xiao Anglong	50	−51	0.14	25	−11	0.99	228

values than during cold seasons for Ts. Tuyuksu, Kara-Batkak, Sary Tor, Abramov, and Batysh Sook glaciers in the Tien Shan (Table 3). Annual mass-balance variations from 1970 to 2019 for Xiao Anglong Glacier in western Tibet were mainly controlled by variations in mass balance during ablation seasons (Table 3, Zhu et al., 2021b). Considering the major role of the differences in precipitation seasonality between glaciers in western Tibet and the western Tien Shan, and the importance of ablation season mass balance variations with respect to their annual mass balance variations for glaciers between western Tibet and the western Tien Shan, analyzing the temporal and spatial variations of ablation season mass balance for glaciers between the two regions are critical for understanding the correlation relationships of mass balance variations between these two regions.

Fig. 2 shows that high (or low) ablation season glacier mass balance values in the selected region of the western Tien Shen are matched by low (or high) ablation season glacier mass balance in the selected region of western Tibet. Correlation analysis showed a significant negative correlation for ablation season mass balance during 1970–2019 between (1) Xiao Anglong and Ts. Tuyuksu glaciers ($r = -0.34$, $p < 0.05$, $n = 50$), (2) Xiao Anglong and Kara-Batkak glaciers ($r = -0.52$, $p < 0.05$, $n = 24$), and (3) Xiao Anglong and Abramov glaciers ($r = -0.53$, $p < 0.05$, $n = 32$). Furthermore, a three-year running mean was used for detrended

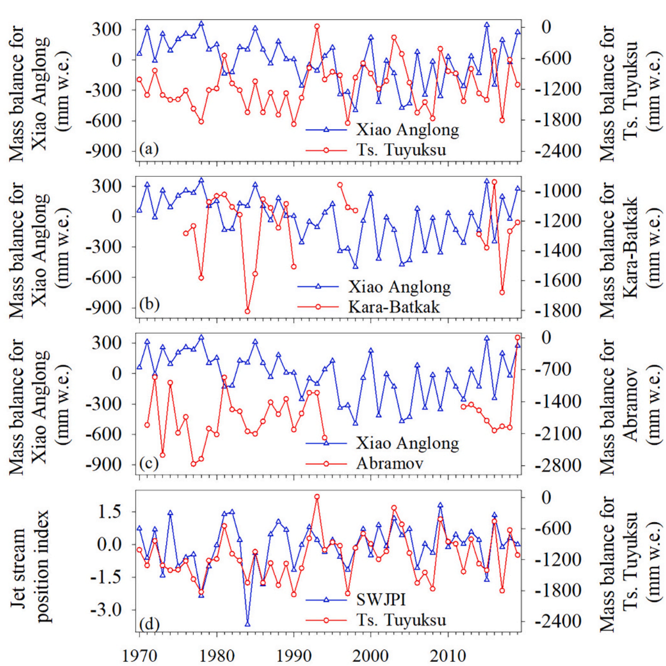

Fig. 2. Comparisons of mass balance of Xiao Anglong Glacier with that of (a) Ts. Tuyuksu, (b) Kara-Batkak and (c) Abramov glaciers during the ablation season from 1970 to 2019. (d) Comparison between the mass balance of Ts. Tuyuksu Glacier and the subtropical westerly jet position index during the ablation season from 1970 to 2019.

ablation season mass balances on Xiao Anglong and Ts. Tuyuksu glaciers during the period 1970–2019, and the correlation coefficient between them remained negative (−0.46). This correlation coefficient is significant at the 0.05 confidence level, as it is more negative than the critical value of −0.34 defined according to Monte Carlo analysis described in Section 2.3. Notably, ablation season mass balance variations of typical glaciers show a contrast between western Tibet and the western Tien Shan at interannual timescales.

3.3. Relationships between ablation season glacier mass balances in both regions, and seasonal temperature and precipitation

Interannual variability of ablation season mass balance is primarily related to variations in ablation season air temperature and ablation season precipitation, as stated above. After detrending, our correlation analysis showed that ablation season mass balances for Xiao Anglong Glacier during 1970-2019 exhibited slight negative correlations with ablation season air temperature in western Tibet (30.5–34.5°N, 80–85°E), but significant positive correlations with ablation season precipitation in western Tibet (Fig. 3). Zhu et al. (2021b) reported that ablation season precipitation was a primary driver for fluctuations in annual glacier mass balance in western Tibet because ablation season precipitation greatly influences accumulation processes by changing snowfall, and ablation processes by changing glacier surface albedo (Fujita and Ageta, 2000). Fluctuations in annual glacier mass balance mainly occur during the ablation season (Zhu et al., 2021b). Thus, such interannual variations in ablation season mass balance of glaciers in the selected region of western Tibet are mainly controlled by variations in ablation season precipitation.

After detrending, ablation season mass balances for Ts. Tuyuksu Glacier, Kara-Batkak Glacier, and Abramov Glacier (Fig. 4 and Figs. S4-S5) showed significant negative correlations with ablation season air temperature in the western Tien Shan, as well as showing a significant positive correlation with ablation season precipitation in the western Tien Shan during 1970–2019. The absolute values of correlation coefficients between ablation season mass balance and ablation season air temperature for these three glaciers were slightly higher than those between ablation season mass balance and ablation season precipitation (Fig. 4 and Figs. S4-S5). Among the three studied glaciers in the western Tien Shan, only Ts. Tuyuksu Glacier showed a weak positive relationship between ablation season mass balances and cold season precipitation. Thus, ablation season glacier mass balance variations in the selected region of the western Tien Shan are controlled by ablation season air temperature, and to a lesser extent, ablation season precipitation.

4. Discussion

4.1. Causes of correlations between reconstructed glacier mass balance data and climate drivers

Some studies have shown that variations in mass balance of glaciers are mainly controlled by climatic factors, such as air temperature and

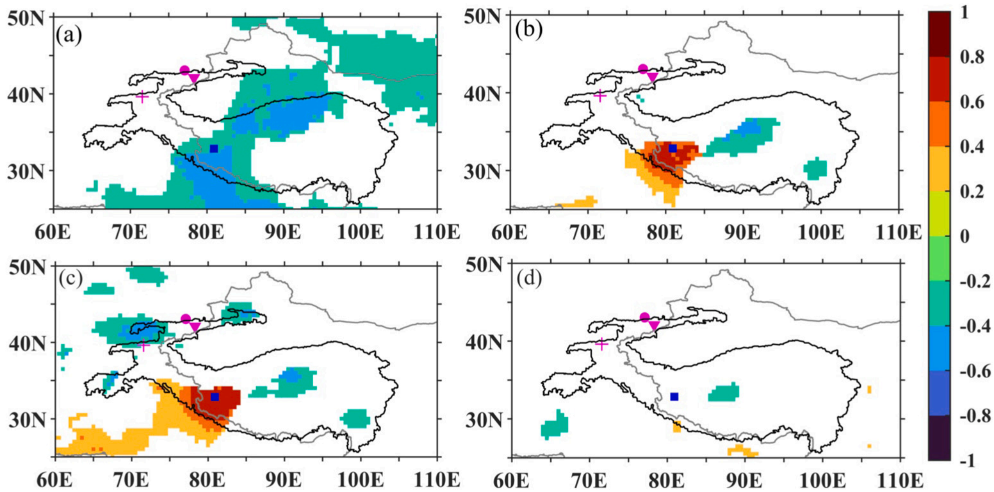

Fig. 3. Spatial distribution of correlation coefficients from 1970 to 2019 determined using correlation analysis between detrended ablation season mass balance on Xiao Anglong Glacier and (a) detrended CRU gridded ablation season air temperature data, (b) detrended CRU gridded annual precipitation data, (c) detrended CRU gridded ablation season precipitation data, and (d) detrended CRU gridded cold season precipitation data. Only significant correlations ($p < 0.05$) are shown on all figures. Symbols are as follows: pink dot, Ts. Tuyuksu Glacier; pink inverted triangle, Kara-Batkak Glacier; pink cross, Abramov Glacier; blue square, Xiao Anglong Glacier. (For interpretation of the references to colour in this figure legend, the reader is referred to the web version of this article.)

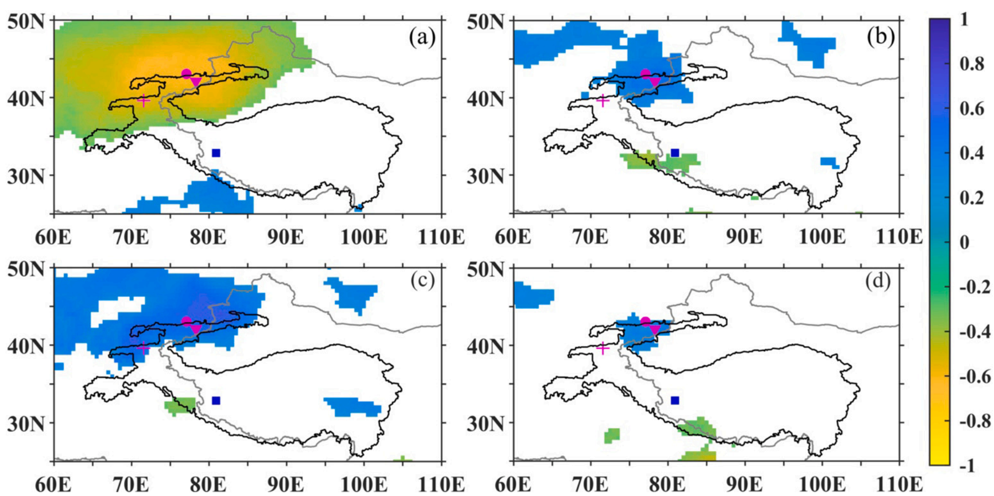

Fig. 4. Spatial distribution of correlation coefficients from 1970 to 2019 using correlation analysis between detrended ablation season mass balance on Ts. Tuyuksu Glacier and (a) detrended CRU gridded ablation season air temperature data, (b) detrended CRU gridded annual precipitation data, (c) detrended CRU gridded ablation season precipitation data, and (d) detrended CRU gridded cold season precipitation data. Only significant correlations ($p < 0.05$) are shown on all figures. Symbols are as follows: pink dot, Ts. Tuyuksu Glacier; pink inverted triangle, Kara-Batkak Glacier; pink cross, Abramov Glacier; blue square, Xiao Anglong Glacier. (For interpretation of the references to colour in this figure legend, the reader is referred to the web version of this article.)

precipitation (Oerlemans and Reichert, 2000; Oerlemans, 2005; Zhu et al., 2018, 2022a). In addition, the measured mass balance time series for Urumqi Glacier No.1 in eastern Tien Shan and Qiyi Glacier in the Qilian Mountains showed significant negative correlations at interannual timescales with the measured air temperature at the Daxigou meteorological station and the Tuole meteorological station, respectively (Wang et al., 2010; Wang et al., 2016; Zhu et al., 2022a). Xiao Dongkemadi Glacier in the Tanggula Mountains showed a similar phenomenon, the correlation coefficient between the measured annual mass balance and the measured ablation season air temperature (or annual precipitation) at Anduo meteorological station was −0.75 (or 0.42) during 1989-2010. Thus, our data show direct correlations between glacier mass balances and local/regional climate drivers (i.e. air temperature and precipitation) in the TP.

The TP notably lacks long-term in situ measurements of glacier mass balance due to significant differences in regional climates. As such, a continuous seasonal time series of glacier mass balance has been simulated across the TP in order to study the relationships between climate drivers (atmospheric circulation, precipitation, and air temperature) and glacier variations. This allows the impact of climate change on regional glacier meltwater release to be analyzed, among other phenomena (Barandun et al., 2015, 2020; Farinotti et al., 2015; Mölg et al., 2014; Yang et al., 2016; Zhu et al., 2018, 2021b). In addition, simulations of annual mass balance time series for some glaciers in the TP match well with observations (Barandun et al., 2015; Yang et al., 2016; Zhu et al., 2021b, 2022a). For example, a correlation coefficient of 0.92 ($p < 0.01$, $n = 20$ and RMSE = 162 mm w.e.) was determined between modelled and measured mass balances for Qiyi Glacier, and modelled mass balance was also shown to have a significant negative correlation with ablation season air temperature (Zhu et al., 2022a). These results show that reconstructed glacier mass balances can be used to indicate some changes in a glacier's characteristics at the regional/local scale, especially when a long-term glacier mass balance time series is incomplete. Nonetheless, this requires input variables to be of a high quality and that glacier model is calibrated using more measured values, such as in-situ measurements of glacio-meteorological data and discharge data, and snowline observations and glacier thickness changes derived from satellite imagery. Meteorological data for Xiao Anglong Glacier is of a high quality and its reconstructed values largely agree with in situ observations of mass balance (Zhu et al., 2022a). Therefore, we consider it suitable to use for discussion of correlations between reconstructed glacier mass balance time series and climate drivers (i.e. air temperature and precipitation) in this work.

4.2. Impacts of atmospheric circulation on opposing ablation season mass balance variations between glaciers in western Tibet and the western Tien Shan

The above-described opposing variations in regional glacier mass balance during the ablation season may be linked to large-scale atmospheric circulation patterns, which drive the variations in air temperature and precipitation during ablation seasons. Following the method of Zhu et al. (2021b), we found that ablation season subtropical westerly jet position index (SWJPI) is negatively correlated with ablation season mass balance (with detrending, $r = -0.4$, $p < 0.05$), because variations in ablation season SWJPI affect ablation season precipitation in western Tibet. The ablation season SWJPI showed a positive correlation with ablation season mass balance for Ts. Tuyuksu ($r = 0.58$, $p < 0.05$, $n = 50$, Kara-Batkak ($r = 0.58$, $p < 0.05$, $n = 24$), and Abramov ($r = 0.61$, $p < 0.05$, $n = 32$) glaciers situated in the western Tien Shan from 1970 to 2019 (Fig. 2). To understand how the variations in SWJPI relates to a variable response in ablation season glacier mass balance for the two areas, we further analyzed the spatial correlations between ablation season SWJPI and CRU ablation season air temperature and precipitation from 1970 to 2019 (Fig. 5). Ablation season SWJPI values show significant and negative relationships with ablation season air temperature in the western Tien Shan, but show no significant relationships with ablation season air temperature in western Tibet, By contrast, SWJPI show significant and positive correlations with ablation season precipitation in the western Tien Shan, but significant and negative relationships with ablation season precipitation in western Tibet. In addition, regionally averaged ablation season air temperature and precipitation show no significant correlation in western Tibet (30.5–34.5°N, 80–85°E), but a significant negative relationship in the western Tien Shan (39.25–43.25°N, 71.25–79.25°E, after detrending, $r = -0.51$, $p < 0.01$) (Fig. S6). These relationships show that changes in ablation season subtropical westerly jet position can impact ablation season air temperature and precipitation in the western Tien Shan, and ablation season precipitation in western Tibet.

To consider these relationships between SWJPI, air temperature, and precipitation for the ablation season, we examined the correlations between SWJPI and the 300 hPa and 600 hPa geopotential height and wind fields. Fig. 6a and b show different centers of anomalies in atmospheric circulation above the northern Atlantic Ocean, Europe, Central Asia, the

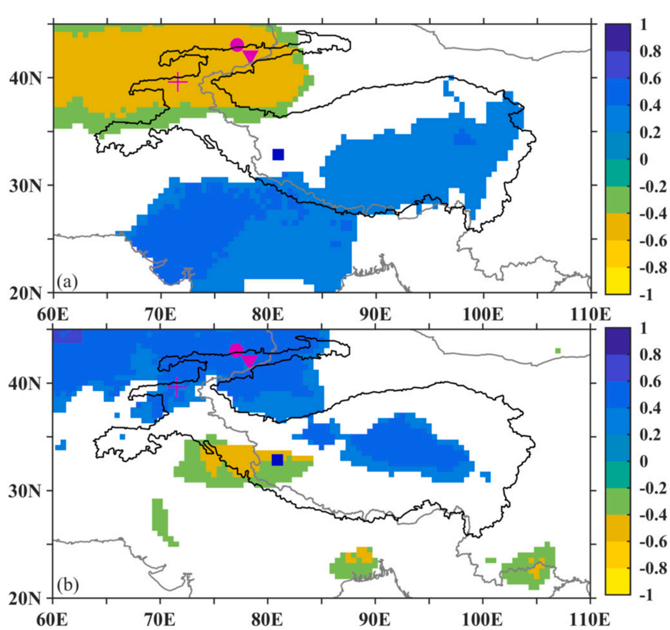

Fig. 5. Correlation fields between detrended ablation season subtropical westerly jet position index and detrended CRU gridded ablation season (a) air temperature and (b) precipitation from 1970 to 2019. Only significant correlations ($p < 0.05$) are plotted. Symbols are as follows: pink dot, Ts. Tuyuksu Glacier; pink inverted triangle, Kara-Batkak Glacier; pink cross, Abramov Glacier; blue square, Xiao Anglong Glacier. (For interpretation of the references to colour in this figure legend, the reader is referred to the web version of this article.)

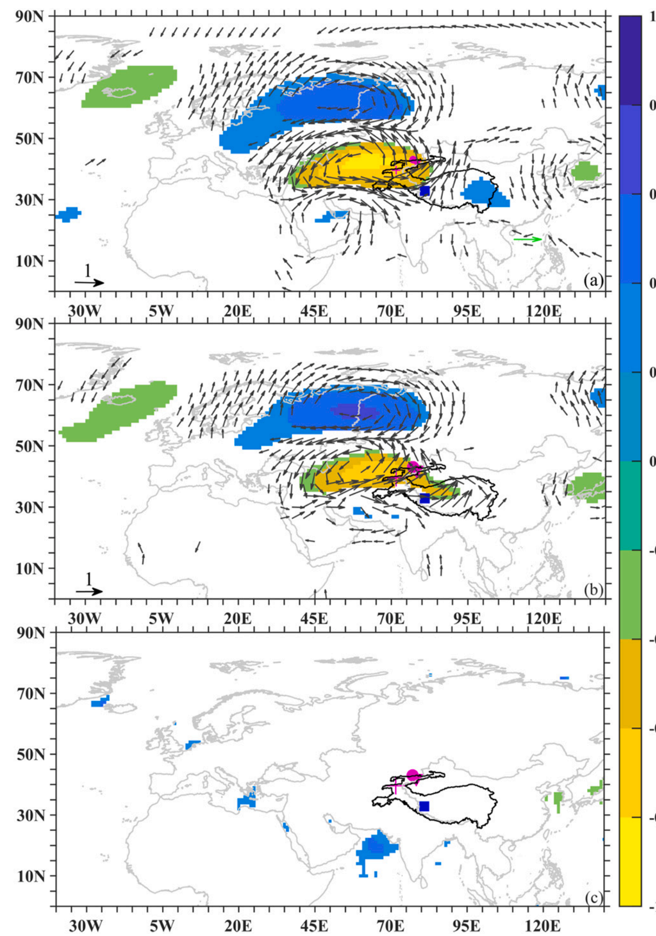

Fig. 6. Correlation analysis of the subtropical westerly jet position index with (a) 300 hPa, and (b) 600 hPa geopotential height (gpm) and wind fields, and (c) sea surface temperature during the ablation season from 1970 to 2019. All data are detrended. Only significant correlations ($p < 0.05$) are shown on all figures. Vectors in a and b are composites of the correlations with horizontal wind components (zonal and meridional wind speed): a significant vector denotes either one of its components is significant. The geopotential height and wind fields are from the JRA55 dataset. SST data are from the HadISST dataset. Symbols are as follows: pink dot, Ts. Tuyuksu Glacier; pink inverted triangle, Kara-Batkak Glacier; pink cross, Abramov Glacier; blue square, Xiao Anglong Glacier. (For interpretation of the references to colour in this figure legend, the reader is referred to the web version of this article.)

region north of the Arabian Sea, and East Asia at 300 hPa and 600 hPa, respectively. The geopotential height and anticyclonic anomaly for 300 hPa are high at high latitudes over Europe, and low over Central Asia, indicating a southward shift of the upper-tropospheric westerlies and the subtropical westerly jet stream (Mölg et al., 2017; Zhu et al., 2021b). In addition, higher geopotential heights and anticyclonic anomalies for 300 hPa that occurred north and northwest of the Arabian Sea may also favor a southward shift of the subtropical westerly jet (Zhao et al., 2018).

The strong northerly wind anomaly that extends from high latitudes to the subtropics, and the enhanced westerlies that occur at 30–35°N, favor the advection of cold and dry air to northwest India and western Tibet (Mölg et al., 2017, Fig. 6a and b). This circulation pattern can reduce precipitation by reducing the transport of moist air from central-eastern India, which decreases convective instability over western Tibet (Zhu et al., 2021b). Cold and dry air also reduces cloud cover, which enhances incoming shortwave radiation and thereby larger surface net radiations, and may increase air temperature during the ablation season in western Tibet (Kononova et al., 2015; Li et al., 2021). Warming trends can also increase ablation season air temperature in western Tibet (Zhu et al., 2021a). Reduced air temperature relating to a southward shift of the subtropical westerly jet (Mölg et al., 2017) may be counteracted by increases in air temperature driven by reduced cloud cover and the warming trend (Kononova et al., 2015; Li et al., 2021; Zhu et al., 2021b). Hence, ablation season air temperature in western Tibet does not show a relationship with ablation season SWJPI.

Ablation season precipitation over the western Tien Shan is modulated primarily by moisture transport in the lower–middle troposphere (i.e. 600 hPa, Dong et al., 2018). At 600 hPa (Fig. 6b), an anticyclonic anomaly over the northern part of the northern Arabian Sea and a cyclonic anomaly over Central Asia result in enhanced southerly flow in the western flank of the anticyclonic anomaly and increased westerly winds in the southern flank of the cyclonic anomaly. This configuration allows the Tien Shan to receive more atmospheric moisture from the Indian Ocean (Zhao and Zhang, 2016), and Mediterranean Ocean, and Black Sea (Aizen et al., 2004; Dong et al., 2018). Meanwhile, the western Tien Shan and eastern Pamir Mountains experience southerly wind anomalies on the eastern flank of the cyclonic anomaly over Central Asia at 300 hPa and 600 hPa (Fig. 6a and b). This flow reduces the strength of upper tropospheric westerlies in the western Tien Shan and eastern Pamir Mountains, which facilitates the development of regional convection (Mölg et al., 2017) and regional moisture accumulation. These circulation patterns set up conditions that promote high precipitation during the ablation season over the western Tien Shan. Formation of a cyclonic anomaly over Central Asia (Fig. 6a and b) seems to be a major factor that causes surface cooling of the western Tien Shan (Mölg et al., 2017; Zhao et al., 2014). In addition, high precipitation rates are associated with high cloud cover, which can reduce incoming solar radiation, thereby further reducing air temperature in the western Tien Shan during the ablation season. This feedback is supported by significant negative correlations between total cloud cover and air temperature over the most areas of the TP during the summer (Ma et al., 2021).

4.3. Processes affecting the subtropical westerly jet position variations

Subtropical westerly jet position variations may be associated with two teleconnection patterns. The first process could be linked to a European–Asian teleconnection. The anticyclonic anomaly over Europe and the cyclonic anomaly over Central Asia at 300 hPa (Fig. 6a) are components of the global wave train sometimes referred to as the Silk Road pattern (Lu et al., 2002; Enomoto et al., 2003; Ding and Wang, 2005; Hong et al., 2018; Mölg et al., 2017; Yasui and Watanabe, 2010). The first process is confirmed by correlations between the 300 hPa regionally averaged geopotential height over Europe (55°–68°N, 35°E–70°E), and the 300 hPa geopotential height and wind fields in the ablation season during 1970-2019, which show wave trains from Europe to Central Asia and northern-central China (Fig. S7). This illustrates that changes in the global wave train or Silk Road pattern can affect the position of the subtropical westerly jet. After detrending, the SWJPI showed a strong correlation with the GTI ($r = -0.58$, $p < 0.005$) and the Silk Road pattern index ($r = -0.48$, $p < 0.005$) in the ablation season during 1970-2019.

The second process involves teleconnections from the Arabian Sea to Central Asia (Fig. 6a and b), which may be related to SST over the Arabian Sea (Zhao and Zhang, 2016). Ablation season SWJPI is positively correlated with SST over the northern Arabian Sea (Fig. 6c). After detrending, the correlation coefficient between ablation season SWJPI and regionally averaged SST over the northern Arabian Sea (15.5°–23.5°N, 60°E–70°E) from 1970 to 2019 was 0.36 ($p < 0.05$, $n = 50$). In addition, correlations between regionally averaged SST over the northern Arabian Sea, and the 300 hPa and 600 hPa geopotential height and wind fields in the ablation season, indicate that high SST values in the Indian Ocean cause anomalous anticyclone at 600 hPa over the Indian continent monsoon region, alongside an anomalous cyclone at 300 hPa over Central Asia (Fig. S8). Zhao et al. (2018) suggested that these circulation patterns were caused by SST warming over the Indian Ocean, and that such circulations could favor the southward movement of the subtropical westerly jet.

In addition, an anticyclonic anomaly forms at 300 hPa over Europe and a cyclonic anomaly forms over Central Asia (Fig. 6a), which together indicate a southward shift of the upper-tropospheric westerlies (Mölg et al., 2017). An anticyclone over the Arabian Sea (Fig. S8b) formed due to increased SST over the Indian Ocean, indicating weakening of the South Asian monsoon (Zhao et al., 2018). Thus, these results suggest that interactions between the monsoon and westerlies impact the position of the subtropical westerly jet.

4.4. Limitations and uncertainties of the mass balance data

In this work, we compared ablation season mass balance variations of four glaciers situated in two geographical regions; however, these ablation season mass balance variations are affected by various factors that may generate different sources of uncertainty for the results in this work. As such, we outline the limitations and uncertainties of our data.

Firstly, the data used for glacier mass balance variations carries inherent uncertainty. Mass balance of Ts. Tuyuksu, Abramov, and Kara-Batkak glaciers were determined using in-situ measurements taken during the ablation season and the cold season each year using glaciological methods. For these glaciers, the uncertainties of annual surface mass balances lie within the range 200–300 mm w.e. a^{-1} (Barandun et al., 2018; Kenzhebaev et al., 2017), and are derived from uncertainties in point measurements, uncertainties related to the representativeness of the point measurements, and uncertainties associated with the method used to extrapolate point measurements into estimations of the glacier's entire surface area. Mass balance for Xiao Anglong Glacier during ablation seasons used modelled values, which themselves have uncertainties of 149–370 mm w.e. a^{-1} (Barandun et al., 2020; Zhu et al., 2021b, 2022a). Nonetheless, the effect that such uncertainties have on interannual variations in a glacier's mass balance is unclear. Recent studies have shown that measured or modelled mass-balance time series could be used to monitor variations in climate, atmospheric circulation, and glacial meltwater (Barandun et al., 2020; Mölg et al., 2014; Zhu et al., 2021b, 2022a). This indicates that the influence of the above-mentioned uncertainties on interannual variations in mass balance is small.

Secondly, non-climatic factors can affect glacier mass balance variations, such as differences in topography, the degree of debris-covered conditions, and glacier surges (Bhattacharya et al., 2021; Zhu et al., 2018, 2022b). Glacier topography may enhance mass balance variations that are caused by climate change (Liu and Liu, 2016; Zhu et al., 2022b); for example, while each glacier in the same region has a unique topography, mass balance variations in each will still be similar. Additionally, some studies have reported that clean-ice and debris-covered glaciers experience similar rates of mass loss at interdecadal timescales (Maurer et al., 2021). Considering that most glaciers in the Tien Shan are clean-ice glaciers (not covered by debris) and debris-covered glaciers can lose mass at a similar rate to debris-free glaciers, Farinotti et al. (2015) modelled glacier mass balances across the Tien Shan without separating debris-free and debris-covered surfaces. These indicate that variations in mass balance of debris-covered glaciers are similar to those of clean-ice glaciers in the same climate region. Western Tibet and the western Tien Shan host a small number of surge-type glaciers, and there is no significant difference in mass balance between surge-type and non-surge-type glaciers (Guillet et al., 2022). Thus, we expect that the above-mentioned non-climatic factors should not cause notable differences in mass balance variations between glaciers in the same climate region.

Thirdly, we note that climate is the dominant driving force for variations in glacier mass balance across the TP (Barandun et al., 2020; Yao et al., 2022; Zhu et al., 2022a). Some previous studies have shown that the values of glacier mass balance variations caused by the same climate change in the same region spatially differ; however, interannual variations in glacier mass balance are similar within the same region. For example, this effect has been noted for glaciers in the Nyainqentanglha Mountains, the Qilian Mountains, and the western Tien Shan, with this relationship being stronger when multiple glaciers are located close to each other (Table 2; Barandun et al., 2020; Liu and Liu, 2016; WGMS, 2021; Yu et al., 2013; Zhu et al., 2022b). Glaciers in the western Tien Shan show large accumulations during the cold season, which can affect their annual mass balance variations. As described in Section 3.1, the strong winds and pronounced differences in surface topography can generate different cold season mass balance variations for glaciers in the same region due to variable snowdrift; however, mass balance variations of the studied glaciers during the ablation season are more similar to those situated in the western Tien Shan, due primarily to similar variations in ablation ablation-season air temperature and precipitation. Thus, we assumed in this work that interannual variations in ablation season mass balance for glaciers in the selected region in the western Tien Shan were similar.

However, there are few glaciers in the two regions, which have measured long-term ablation season mass balance data and meteorological data. Conclusions derived from such low spatial resolution datasets would carry relatively high uncertainty, and there would be limits to modelling the spatial patterns of ablation season mass balances for glaciers in these two regions at annual timescales. An expanded network of glacier-monitoring systems in these regions is needed to produce more reliable results. Considering the difficulties involved with conducting in-situ measurements, satellite, and airborne remote sensing data are crucial for monitoring glaciers over long-term periods of 5 to 10 years (Barandun et al., 2020; Bhattacharya et al., 2021; Yao et al., 2022). Higher resolution temporal and spatial remote sensing data should be combined with independent data sources to assess glacier mass balance variations at interannual timescales. Regional climate models, such as the Advanced Research Weather Research and Forecasting model (WRF), have been used to simulate climate conditions within the TP (Maussion et al., 2014), and have improved over time such that they can now realistically predict climate changes in the TP (Ou et al., 2020). In addition, glacier models involving complicated physical processes have been developed to better simulate glacier mass balance variations under different conditions across the TP (Barandun et al., 2021; Zekollari et al., 2022; Zhu et al., 2022a). Thus, by combining more in-situ observations, improved spatial and temporal remote sensing data, and numerical models, future studies will be able to further investigate regional-scale glacier mass balance variations at annual to seasonal timescale within the TP, and reduce the uncertainties associated with this work (Barandun et al., 2020; Yao et al., 2022; Zhu et al., 2022b).

4.5. Comparison with other studies

Investigating the major forces that drive glacier mass balance variations within the TP is important for predicting future changes in glacier characteristics, and their associated effects on environmental and social issues (e.g. water resources). Some previous studies have found that the variations in mass balance of glaciers are mainly controlled by climate factors (Oerlemans, 2005; Zhu et al., 2018, 2022a). The climate-related driving forces for glacier mass balance variations in the Tien Shan and Pamir-Alay are complex (Barandun and Pohl, 2022). Thus, we mainly compared our results with previous studies conducted in these regions. For Abramov Glacier in the eastern parts of the Pamir-Alay, annual precipitation plays a more important role in interannual mass balance variations than ablation season air temperature (Kronenberg et al., 2022). According to the climate data reported by Kronenberg et al. (2022) and measured mass balance data for Abramov Glacier (WGMS, 2021), correlation coefficients between ablation season mass balance and ablation season air temperature and between ablation season mass balance and ablation season precipitation during 1970-2019 were −0.79 and 0.68 ($n = 32$, $p < 0.05$), respectively. These results highlight that the relative importance of climate drivers for mass balance variations between annual and ablation season timescales differ slightly for this glacier, which is likely due to the important contribution of cold season accumulation to the glacier's annual mass balance. The results of our work (Fig. S5) agree with those of the above-mentioned study, indicating that ablation season air temperature plays a slightly more important role in controlling interannual variations in ablation season mass balance than ablation season precipitation. In addition, during an investigation of the driving forces of regional glacier annual mass balance variations in the Tien Shan and Pamir-Alay, Barandun and Pohl (2022) reported that air temperature was more important than precipitation for the eastern and northern/western Tien Shan and to some degree also for the central Tien Shan. Furthermore, based on tree ring data, Zhang et al. (2019) found that mass balance variations of Ts. Tuyuksuy Glacier in the western Tien Shan were controlled by a combination of summer air temperature and annual precipitation conditions across Central Asia during the past 115 years (1901-2014). And the correlation between annual mass balance and summer air temperature was stronger than that between annual mass balance and annual precipitation (Zhang et al., 2019). These findings and the results of our work show that ablation season glacier mass balance variations in the selected region in the western Tien Shan may be related to variations in ablation season air temperature and ablation season precipitation at interannual timescales, and that ablation season air temperature is slightly more influential than ablation season precipitation in such cases.

Atmospheric circulation can affect glacier mass balance variations by altering the climate in a region (Mölg et al., 2014; Yao et al., 2022; Zhu et al., 2021b, 2022b). Specifically, precipitation change driven by zonal and meridional atmospheric circulation patterns can affect glacier mass balance variations in Central Asia (Aizen et al., 2001). A stronger meridional component of atmospheric circulation from the south promotes precipitation in Central Asia, which can increase mass balance for glaciers in the Tien Shan (Aizen et al., 2001) and eastern Pamir (Zhu et al., 2018). Farinotti et al. (2015) reported a positive correlation in the Tien Shan between regionally averaged annual glacier mass balance and regionally averaged summer meridional wind speed in the middle and upper troposphere. Here, we also identified a southerly wind anomaly that caused higher mass balance in the selected region of the western Tien Shan (Fig. 6). Alongside precipitation, air temperature is affected by changing atmospheric circulation and also contributes to mass balance variations in the western Tien Shan. Kononova et al. (2015) reported that intense mass loss of Ts. Tuyuksu Glacier in the western Tien Shan may be related to the anticyclonic circulation patterns accompanied by relatively high air temperature and low precipitation during summer; and when a cyclonic circulation pattern forms over the region during summer, air temperature decreases and precipitation increases, which results in a relatively high mass balance. These studies support the results presented here, whereby such cyclones (anticyclones) are accompanied by relatively high (low) mass balance and corresponding climate conditions during ablation seasons in the selected region of the western Tien Shan.

5. Conclusion

This study investigated ablation season glacier mass balance differences between western Tibet and the western Tien Shan during 1970-2019 and associated key atmospheric circulation patterns at interannual timescales. We showed that ablation season mass balance variations were related to ablation season air temperature and ablation season precipitation in the western Tien Shan and were mainly controlled by ablation season precipitation in western Tibet at interannual timescales. Further analysis suggested that ablation season mass balance variations of glaciers in the western Tien Shan were opposite to those in western Tibet at interannual timescales. The contrasting responses of mass balance in the two areas were directly related to changes in the subtropical westerly jet position during the ablation season. When the subtropical westerly jet moves southward, the western Tien Shan shows higher ablation season precipitation and lower air temperature which contributes to higher mass balance, whereas western Tibet experiences lower ablation season precipitation, causing lower mass balance. When the subtropical westerly jet moves northward, the above processes are reversed. The changes in the subtropical westerly jet position can be influenced by both atmospheric circulation in Europe, through a European–Asian teleconnection, and to SSTs in the northern Arabian Sea, through Central-Asia–tropical-Indian-Ocean teleconnection. In other words, interactions between the South Asian monsoon and the mid-latitude westerlies impact the position of the subtropical westerly jet, which causes opposite ablation season mass balance variations between glaciers in western Tibet and the western Tien Shan by controlling regional climate change. Results from this work increased our understanding of the spatiotemporal variability of glacier mass balance in the TP. More glaciers will be explored in the future to find whether the correlations of mass balance variations can be detected in other climatic regions of the TP based on long-term measured (Barandun et al., 2020; Wagnon et al., 2013; Yao et al., 2012) and modelled (Mölg et al., 2014) seasonal glacier mass balance data.

Declaration of Competing Interest

The authors declare that they have no known competing financial interests or personal relationships that could have appeared to influence the work reported in this paper.

Data availability

Data will be made available on request.

Acknowledgments

We acknowledge the staff at the Ngari Station for Desert Environment Observation and Research, Institute of Tibetan Plateau Research, Chinese Academy of Sciences, for help in the field. This study is jointly funded by the Strategic Priority Research Program of Chinese Academy of Sciences (Grant No. XDA2006020102), the Second Tibetan Plateau Scientific Expedition and Research Program (Grant No. 2019QZKK0201), National Natural Science Foundation of China (Grant No. 41971092, 4191101270 and 41771085), National Key Research and Development Project (2019YFC1509102), and National Science Foundation Paleo Perspectives on Climate Change (Award 1502919). JRA-55 data and CRU data were obtained from https://jra.kishou.go.jp/JRA-55/index_en.html and http://www.cru.uea.ac.uk/data/, respectively. We thank the two reviewers for their valuable comments. The mass balance data for glaciers in the western Tien Shan can be downloaded from the world glacier monitoring service (https://wgms.ch/data_databaseversions/). Any other specific data can be provided by the authors upon request.

Appendix A. Supplementary data

Supplementary data to this article can be found online at https://doi.org/10.1016/j.gloplacha.2022.103997.

References

Aizen, V.B., Aizen, E.M., Melack, J.M., Dozier, J., 1997. Climatic and hydrologic changes in the Tien Shan, Central Asia. J. Climate 10, 1393–1404. https://doi.org/10.1175/1520-0442(1997)010<1393:cahcit>2.0.co;2.

Aizen, E.M., Aizen, V.B., Melack, J.M., Nakamura, T., Ohta, T., 2001. Precipitation and atmospheric circulation patterns at mid-latitudes of Asia. Int. J. Climatol. 21, 535–556. https://doi.org/10.1002/joc.626.

Aizen, V.B., Aizen, E.M., Melack, J.M., Kreutz, K.J., Cecil, L.D., 2004. Association between atmospheric circulation patterns and firn-ice core records from the Inilchek glacierized area, central Tien Shan. Asia. J. Geophys. Res. Atmos. 109, D08304. https://doi.org/10.1029/2003JD003894.

Azam, M.F., Srivastava, S., 2020. Mass balance and runoff modelling of partially debris-covered Dokriani Glacier in monsoon-dominated Himalaya using ERA5 data since 1979. J. Hydrol. 590, 125432 https://doi.org/10.1016/j.jhydrol.2020.125432.

Azisov, E., Hoelzle, M., Vorogushyn, S., Saks, T., Usubaliev, R., Esenaman Uulu, M., Barandun, M., 2022. Reconstructed centennial mass balance change for Golubin Glacier, Northern Tien Shan. Atmosphere 13, 954. https://doi.org/10.3390/atmos13060954.

Barandun, M., Pohl, E., 2022. Central Asia's spatiotemporal glacier response ambiguity due to data inconsistencies and regional simplifications. Cryosphere Discuss. 1–34. https://doi.org/10.5194/tc-2022-117. Submitted for publication.

Barandun, M., et al., 2015. Re-analysis of seasonal mass balance at Abramov glacier 1968–2014. J. Glaciol. 61, 1103–1117. https://doi.org/10.3189/2015JoG14J239.

Barandun, et al., 2018. Multi-decadal mass balance series of three kyrgyz glaciers inferred from modelling constrained with repeated snow line observations. Cryosphere 12, 1899–1919. https://doi.org/10.5194/tc-12-1899-2018.

Barandun, M., Fiddes, J., Scherler, M., Mathys, T., Saks, T., Petrakov, D., Hoelzle, M., 2020. The state and future of the cryosphere in Central Asia. Water Security 11, 100072. https://doi.org/10.1016/j.wasec.2020.100072.

Barandun, M., et al., 2021. Hot spots of glacier mass balance variability in Central Asia. Geophys. Res. Lett. 48 https://doi.org/10.1029/2020GL092084 e2020GL092084.

Bazai, N.A., et al., 2020. Increasing glacial lake outburst flood hazard in response to surge glaciers in the Karakoram. Earth-Sci. Rev. 212, 103432 https://doi.org/10.1016/j.earscirev.2020.103432.

Bhattacharya, A., et al., 2021. High Mountain Asian glacier response to climate revealed by multi-temporal satellite observations since the 1960s. Nat. Commun. 12, 4133. https://doi.org/10.1038/s41467-021-24180-y.

Brun, F., Berthier, E., Wagnon, P., Kääb, A., Treichler, D., 2017. A spatially resolved estimate of High Mountain Asia glacier mass balances from 2000 to 2016. Nat. Geosci. 10, 668–673. https://doi.org/10.1038/ngeo2999.

Chen, F., et al., 2019. Westerlies Asia and monsoonal Asia: Spatiotemporal differences in climate change and possible mechanisms on decadal to sub-orbital timescales. Earth-Sci. Rev. 192, 337–354. https://doi.org/10.1016/j.earscirev.2019.03.005.

Chen, C., Zhang, X., Lu, H., Jin, L., Du, Y., Chen, F., 2020. Increasing summer precipitation in arid Central Asia linked to the weakening of the East Asian summer monsoon in the recent decades. Int. J. Climatol. 41, 1024–1038. https://doi.org/10.1002/joc.6727.

Cook, K., Andermann, C., Gimbert, F., Adhikari, B.R., Hovius, N., 2018. Glacial lake outburst floods as drivers of fluvial erosion in the Himalaya. Science 362, 53–57. https://doi.org/10.1126/science.aat4981.

Di Lorenzo, E., Cobb, K.M., Furtado, J.C., Schneider, N., Anderson, B.T., Bracco, A., Alexander, M.A., Vimont, D.J., 2010. Central Pacific El Niño and decadal climate change in the North Pacific. Nature Geosci. 3, 762–765. https://doi.org/10.1038/ngeo984.

Dikikh, A.N., 1982. The Regime of Modern Glaciation of the Central Tien Shan. Frunze, 159. Rezhim sovremennogo oledeneniya Tsentral'nogo Tyan'-Shanya, Russian.

Ding, Q., Wang, B., 2005. Circumglobal teleconnection in the Northern Hemisphere summer. J. Climate 18, 3483–3505. https://doi.org/10.1175/JCLI3473.1.

Dong, W., et al., 2018. Regional disparities in warm season rainfall changes over arid eastern–central Asia. Sci. Rep. 8, 13051. https://doi.org/10.1038/s41598-018-31246-3.

Dyurgerov, M.B., 2002. Glacier mass balance and regime: data of measurements and analysis (Occasional Paper 55). Institute of Arctic and Alpine Research, University of Colorado, Boulder, Boulder, CO. https://doi.org/10.7265/N52N506F.

Dyurgerov, M.B., Liu, C., Xie, Z., 1995. Tien Shan Glaciation (Oledenenie Tian Shania). VINITI, Moscow, p. 237 [In Russian].

Enomoto, T., Hoskins, B.J., Matsuda, Y., 2003. The formation mechanism of the Bonin high in August. Quart. J. Roy. Meteor. Soc. 129, 157–178. https://doi.org/10.1256/qj.01.211.

Farinotti, D., et al., 2015. Substantial glacier mass loss in the Tien Shan over the past 50 years. Nature Geosci. 8, 716–722. https://doi.org/10.1038/ngeo2513.

Fujita, K., Ageta, Y., 2000. Effect of summer accumulation on glacier mass balance on the Tibetan Plateau revealed by mass-balance model. J. Glaciol. 46, 244–252. https://doi.org/10.3189/172756500781832945.

Fujita, K., Nuimura, T., 2011. Spatially heterogeneous wastage of Himalayan glaciers. Proc. Natl. Acad. Sci. U.S.A. 108, 14011–14014. https://doi.org/10.1073/pnas.1106242108.

Fujita, K., Takeuchi, N., Nikitin, S.A., Surazakov, A.B., Okamoto, S., Aizen, V.B., Kubota, J., 2011. Favorable climatic regime for maintaining the present-day geometry of the Gregoriev Glacier, Inner Tien Shan. Cryosphere 5, 539–549. https://doi.org/10.5194/tc-5-539-2011.

Gao, J., Risi, C., Masson-Delmotte, V., He, Y., Xu, B., 2016. Southern Tibetan Plateau ice core δ18O reflects abrupt shifts in atmospheric circulation in the late 1970s. Clim. Dynam. 46, 291–302. https://doi.org/10.1007/s00382-015-2584-3.

Glazyrin, G.E., 1985. Distribution and Regime of Mountain Glaciers, Leningrad Gidrometeoizdat, 181. Raspredeleniye i rezhim gornykh lednikov, Russian.

Guillet, G., King, O., Lv, M., Ghuffar, S., Benn, D., Quincey, D., Bolch, T., 2022. A regionally resolved inventory of High Mountain Asia surge-type glaciers, derived from a multi-factor remote sensing approach. Cryosphere 16, 603–623. https://doi.org/10.5194/tc-16-603-2022.

Harada, Y., et al., 2016. The JRA-55 Reanalysis: Representation of atmospheric circulation and climate variability. J. Meteor. Soc. Japan 94, 269–302. https://doi.org/10.2151/jmsj.2016-015.

Harris, I., Osborn, T.J., Jones, P., Lister, D., 2020. Version 4 of the CRU TS Monthly High-Resolution Gridded Multivariate Climate Dataset. Scientific Data 7, 109. https://doi.org/10.1038/s41597-020-0453-3.
Hoelzle, M., et al., 2017. Re-establishing glacier monitoring in Kyrgyzstan and Uzbekistan, Central Asia. Geosci. Instrum. Methods Data Syst. 6, 397–418. https://doi.org/10.5194/gi-6-397-2017.
Hong, X.W., Xue, S.H., Lu, R.Y., Liu, Y.Y., 2018. Comparison between the interannual and decadal components of the Silk Road pattern. Atmos. Oceanic. Sci. Lett. 11, 270–274. https://doi.org/10.1080/16742834.2018.1439661.
Hu, Z., Zhang, C., Hu, Q., Tian, H., 2014. Temperature changes in Central Asia from 1979 to 2011 based on multiple datasets. J. Climate 27, 1143–1167. https://doi.org/10.1175/JCLI-D-13-00064.1.
Hugonnet, R., et al., 2021. Accelerated global glacier mass loss in the early twenty-first century. Nature 592, 726–731. https://doi.org/10.1038/s41586-021-03436-z.
Huss, M., Hock, R., 2018. Global-scale hydrological response to future glacier mass loss. Nat. Clim. Change 8, 135–140. https://doi.org/10.1038/s41558-017-0049-x.
Immerzeel, W.W., et al., 2019. Importance and vulnerability of the world's water towers. Nature 577, 364–369. https://doi.org/10.1038/s41586-019-1822-y.
Kenzhebaev, R., Barandun, M., Kronenberg, M., Chen, Y., Usubaliev, R., Hoelzle, M., 2017. Mass Balance Observations and Reconstruction for Batysh Sook Glacier, Tien Shan, from 2004 to 2016. Cold Regions Sci. Techn. 135, 76–89. https://doi.org/10.1016/j.coldregions.2016.12.007.
Kobayashi, S., et al., 2015. The JRA–55 Reanalysis: General specifications and basic characteristics. J. Meteorol. Soc. Japan 93, 5–48. https://doi.org/10.2151/jmsj.2015-001.
Kononova, N.K., Pimankina, N.V., Yeriskovskaya, L.A., Li, J., Bao, W., Liu, S., 2015. Effects of atmospheric circulation on summertime precipitation variability and glacier mass balance over the Tuyuksu glacier in Tianshan mountains. Kazakhstan. J. Arid Land 7 (5), 687–695. https://doi.org/10.1007/s40333-015-0083-3.
Kronenberg, M., et al., 2016. Mass-balance reconstruction for Glacier No. 354, Tien Shan, from 2003 to 2014. Ann. Glaciol. 57, 92–102. https://doi.org/10.3189/2016AoG71A032.
Kronenberg, M., Machguth, H., Eichler, A., Schwikowski, M., Hoelzle, M., 2021. Comparison of historical and recent accumulation rates on Abramov Glacier, Pamir Alay. J. Glaciol. 67, 253–268. https://doi.org/10.1017/jog.2020.103.
Kronenberg, M., van Pelt, W., Machguth, H., Fiddes, J., Hoelzle, M., Pertziger, F., 2022. Long-term firn and mass balance modelling for Abramov glacier, Pamir Alay. Cryosphere. https://doi.org/10.5194/tc-2021-380. In press.
Li, X.F., Yu, J., Liu, S., Wang, J., Wang, L., 2021. Structure of the Western Tibetan Vortex inconsistent with a thermally-direct circulation. Clim. Dynam. https://doi.org/10.1007/s00382-021-06001-6.
Liu, Q., Liu, S., 2016. Response of glacier mass balance to climate change in the Tianshan Mountains during the second half of the twentieth century. Clim. Dynam. 46, 303–316. https://doi.org/10.1007/s00382-015-2585-2.
Lu, R., Oh, J., Kim, B.J., 2002. A teleconnection pattern in upper-level meridional wind over the North African and Eurasian continent in summer. Tellus A: Dyn. Meteorol. Oceanogr. 54, 44–55. https://doi.org/10.3402/tellusa.v54i1.12122.
Ma, Q., You, Q., Ma, Y., Cao, Y., Zhang, J., Niu, M., Zhang, Y., 2021. Changes in cloud amount over the Tibetan Plateau and impacts of large-scale circulation. Atmos. Res. 249, 105332 https://doi.org/10.1016/j.atmosres.2020.105332.
Makarevich, K.G., 1984. Tuyuksu Glaciers (Northern Tien Shan). Leningrad 171 (Ledniki Tuyuksu (Severnyy Tyan'-Shan)), [In Russian].
Makarevich, K.G., Vilesov, E.N., Shabanov, P.F., 1985. Regime of Glaciers in the Northern Tien Shan for 25 Years (From 1956 to 1981). Data Glaciological Stud. 54, 60–68 (Rezhim lednikov severnogo Tyan'-Shanya za 25 let (s 1956 po 1981), [In Russian].
Mannig, B., et al., 2013. Dynamical downscaling of climate change in Central Asia. Global Planet. Change 110, 26–39. https://doi.org/10.1016/j.gloplacha.2013.05.008.
Marzeion, B., Cogley, J.G., Richter, K., Parkes, D., 2014. Attribution of global glacier mass loss to anthropogenic and natural causes. Science 345, 919–921. https://doi.org/10.1126/science.1254702.
Maurer, J.M., Schaefer, J.M., Rupper, S., Corley, A., 2021. Acceleration of ice loss across the Himalayas over the past 40 years. Sci. Adv. 5 (6), eaav7266. https://doi.org/10.1126/sciadv.aav7266.
Maussion, F., Scherer, D., Mölg, T., Collier, E., Curio, J., Finkelnburg, R., 2014. Precipitation seasonality and variability over the Tibetan Plateau as resolved by the High Asia Reanalysis. Journal of Climate 27, 1910–1927. https://doi.org/10.1175/JCLI-D-13-00282.1.
Mölg, T., Maussion, F., Scherer, D., 2014. Mid-latitude westerlies as a driver of glacier variability in monsoonal High Asia. Nat. Clim. Change 4, 68–73. https://doi.org/10.1038/nclimate2055.
Mölg, T., Maussion, F., Collier, E., Chiang, J.C.H., Scherer, D., 2017. Prominent midlatitude circulation signature in high Asia's surface climate during monsoon. J. Geophys. Res. Atmos. 122, 12702–12712. https://doi.org/10.1002/2017JD027414.
Oerlemans, J., 2005. Extracting a climate signal from 169 glacier records. Science 308, 675–677. https://doi.org/10.1126/science.1107046.
Oerlemans, J., Reichert, B.K., 2000. Relating glacier mass balance to meteorological data by using a seasonal sensitivity characteristic. J. Glaciol. 46, 1–6. https://doi.org/10.3189/172756500781833269.
Ou, T., Chen, D., Chen, X., Lin, C., Yang, K., Lai, H., Zhang, F., 2020. Simulation of summer precipitation diurnal cycles over the Tibetan Plateau at the gray-zone grid spacing for cumulus parameterization. Clim. Dyn. 54, 3525–3539. https://doi.org/10.1007/s00382-020-05181-x.
Pritchard, H.D., 2019. Asia's shrinking glaciers protect large populations from drought stress. Nature 569, 649–654. https://doi.org/10.1038/s41586-019-1240-1.
Pu, J., Yao, T., Yang, M., Tian, L., Wang, N., Ageta, Y., Fujita, K., 2008. Rapid decrease of mass balance observed in the Xiao (Lesser) Dongkemadi Glacier, in the central Tibetan Plateau. Hydrol. Process. 22 (16), 2953–2958. https://doi.org/10.1002/hyp.6865.
Radić, V., Hock, R., 2011. Regionally differentiated contribution of mountain glaciers and ice caps to future sea-level rise. Nature Geosci. 4, 91–94. https://doi.org/10.1038/ngeo1052.
Rayner, N.A., et al., 2003. Global analyses of sea surface temperature, sea ice, and night marine air temperature since the late nineteenth century. J. Geophys. Res. Atmos. 108, 4407. https://doi.org/10.1029/2002JD002670.
Satylkanov, R., 2018. Ablation of Ice and Snow of Kara-Batkak Glacier and its Impact on River Flow. J. Clim. Chang. 4, 1–14. https://doi.org/10.3233/jcc-180009.
Shahgedanova, M., et al., 2018. Changes in the mountain river discharge in the northern Tien Shan since the mid-20th Century: Results from the analysis of a homogeneous daily streamflow data set from seven catchments. J. Hydrol. 564, 1133–1152. https://doi.org/10.1016/j.jhydrol.2018.08.001.
Shi, Y., et al., 2000. Glacier and environment in Chin–now, past and future. Science Press, Beijing, pp. 105–106. In Chinese.
Shi, C., Masson-Delmotte, V., Daux, V., Li, Z., Carré, M., Moore, J.C., 2015. Unprecedented recent warming rate and temperature variability over the east Tibetan Plateau inferred from Alpine treeline dendrochronology. Clim. Dyn. 45, 1367–1380. https://doi.org/10.1007/s00382-014-2386-z.
Shi, H., Li, T., Wei, J., 2017. Evaluation of the gridded CRU TS precipitation dataset with the point raingauge records over the Three-River Headwaters Region. J. Hydrolo. 548, 322–332. https://doi.org/10.1016/j.jhydrol.2017.03.017.
Sorg, A., Bolch, T., Stoffel, M., Solomina, O., Beniston, M., 2012. Climate change impacts on glaciers and runoff in Tien Shan (Central Asia). Nat. Clim. Change 2, 725–731. https://doi.org/10.1038/nclimate1592.
Thompson, L.G., et al., 2018. Ice core records of climate variability on the Third Pole with emphasis on the Guliya ice cap, western Kunlun Mountains. Quat. Sci. Rev. 188, 1–14. https://doi.org/10.1016/j.quascirev.2018.03.003.
Thompson, L.G., Davis, M.E., Mosley-Thompson, E., Porter, S.E., Corrales, G.V., Shuman, C.A., 2021. The impacts of warming on rapidly retreating high-altitude, low-latitude glaciers and ice core-derived climate records. Glob. Planet. Change 203, 103538. https://doi.org/10.1016/j.gloplacha.2021.103538.
Van Tricht, L., Paice, C.M., Rybak, O., Satylkanov, R., Popovnin, V., Solomina, O., Huybrechts, P., 2021. Reconstruction of the Historical (1750-2020) Mass Balance of Bordu, Kara-Batkak and Sary-Tor Glaciers in the Inner Tien Shan. Kyrgyzstan. Front. Earth Sci. 9, 975. https://doi.org/10.3389/feart.2021.734802.
Wagnon, P., et al., 2013. Seasonal and annual mass balances of Mera and Pokalde glaciers (Nepal Himalaya) since 2007. Cryosphere 7, 1769–1786. https://doi.org/10.5194/tc-7-1769-2013.
Wang, N., He, J., Pu, J., Jiang, X., Jing, Z., 2010. Variations in equilibrium line altitude of the Qiyi Glacier, Qilian Mountains, over the past 50 years. Chin. Sci. Bull. 55, 3810–3817. https://doi.org/10.1007/s11434-010-4167-3.
Wang, X., Yang, M., Wan, G., Chen, X., Pang, G., 2013. Qinghai-Xizang (Tibetan) Plateau climate simulation using the regional climate model RegCM3. Climate Res. 57 (3), 173–186. https://doi.org/10.3354/cr01167.
Wang, P., et al., 2016. Analyses of recent observations of Urumqi Glacier No. 1, Chinese Tianshan Mountains. Environ. Earth Sci. 75, 720. https://doi.org/10.1007/s12665-016-5551-3.
Wang, R., Liu, S., Shangguan, D., Radić, V., Zhang, Y., 2019. Spatial heterogeneity in glacier mass-balance sensitivity across High Mountain Asia. Water 11, 776. https://doi.org/10.3390/w11040776.
Wang, P., Li, Z., Li, H., Zhang, Z., Xu, L., Yue, X., 2020. Glaciers in Xinjiang, China: Past changes and current status. Water 12, 2367. https://doi.org/10.3390/w12092367.
WGMS, 2021. Global Glacier Change Bulletin No. 4 (2018-2019). (Vol. 4; M. Zemp et al, Eds.), Zürich: ICSU (WDS)/IUGG(IACS)/UNEP/UNESCO/WMO. World Glacier Monitoring Service. https://doi.org/10.5904/wgms-fog-2021-05.
Yang, W., Guo, X., Yao, T., Zhu, M., Wang, Y., 2016. Recent accelerating mass loss of southeast Tibetan glaciers and the relationship with changes in macroscale atmospheric circulations. Clim. Dynam. 47, 805–815. https://doi.org/10.1007/s00382-015-2872-y.
Yao, T., et al., 2012. Different glacier status with atmospheric circulations in Tibetan Plateau and surroundings. Nat. Clim. Change 2, 663–667. https://doi.org/10.1038/nclimate1580.
Yao, T., et al., 2013. A review of climatic controls on $\delta^{18}O$ in precipitation over the Tibetan Plateau: Observations and simulations. Rev. Geophys. 51, 525–548. https://doi.org/10.1002/rog.20023.
Yao, T., et al., 2019. Recent Third Pole's rapid warming accompanies cryospheric melt and water cycle intensification and interactions between monsoon and environment: Multidisciplinary approach with observations, modeling, and analysis. B. Am. Meteorol. Soc. 100, 423–444. https://doi.org/10.1175/BAMS-D-17-0057.1.
Yao, J., Chen, Y., Yu, X., Zhao, Y., Guan, X., Yang, L., 2020. Evaluation of multiple gridded precipitation datasets for the arid region of northwestern China. Atmos. Res. 236, 104818 https://doi.org/10.1016/j.atmosres.2019.104818.
Yao, T., et al., 2022. The imbalance of the Asian water tower. Nat. Rev. Earth. Environ. https://doi.org/10.1038/s43017-022-00299-4.
Yasui, S., Watanabe, M., 2010. Forcing processes of the summertime circumglobal teleconnection pattern in a dry AGCM. J. Climate 23, 2093–2114. https://doi.org/10.1175/2009JCLI3323.1.
Yu, W., et al., 2013. Different region climate regimes and topography affect the changes in area and mass balance of glaciers on the north and south slopes of the same

glacierized massif (the West Nyainqentanglha Range, Tibetan Plateau). J. Hydrol. 495, 64–73. https://doi.org/10.1016/j.jhydrol.2013.04.034.
Zekollari, H., Huss, M., Farinotti, D., Lhermitte, S., 2022. Ice-Dynamical Glacier Evolution Modeling—A Review. Rev. Geophy. 60 https://doi.org/10.1029/2021RG000754 e2021RG000754.
Zemp, M., et al., 2019. Global glacier mass changes and their contributions to sea-level rise from 1961 to 2016. Nature 568, 382–386. https://doi.org/10.1038/s41586-019-1071-0.
Zhang, R., et al., 2019. A tree ring-based record of annual mass balance changes for the TS. Tuyuksuyskiy Glacier and its linkages to climate change in the Tianshan Mountains. Quaternary Sci. Rev. 205, 10–21. https://doi.org/10.1016/j.quascirev.2018.11.028.
Zhang, G., et al., 2020. Response of Tibetan Plateau lakes to climate change: Trends, patterns, and mechanisms. Earth Sci. Rev. 208, 103269 https://doi.org/10.1016/j.earscirev.2020.103269.
Zhang, H., Li, Z., Zhou, P., 2021. Mass balance reconstruction for Shiyi Glacier in the Qilian Mountains, Northeastern Tibetan Plateau, and its climatic drivers. Clim. Dynam. 56, 969–984. https://doi.org/10.1007/s00382-020-05514-w.
Zhao, T., Fu, C., 2006. Comparison of products from ERA-40, NCEP-2, and CRU with station data for summer precipitation over China. Adv. Atmos. Sci. 23, 593–604. https://doi.org/10.1007/s00376-006-0593-1.
Zhao, Y., Zhang, H., 2016. Impacts of SST warming in tropical Indian Ocean on CMIP5 model-projected summer rainfall changes over Central Asia. Clim. Dynam. 46, 3223–3238. https://doi.org/10.1007/s00382-015-2765-0.
Zhao, Y., et al., 2014. Impact of the middle and upper tropospheric cooling over central Asia on the summer rainfall in the Tarim Basin. China. J. Climate 27, 4721–4732. https://doi.org/10.1175/JCLI-D-13-00456.1.
Zhao, Y., Yu, X., Yao, J., Dong, X., 2018. Evaluation of the subtropical westerly jet and its effects on the projected summer rainfall over central Asia using multi-CMIP5 models. Int. J. Climatol. 38, e1176–e1189. https://doi.org/10.1002/joc.5443.
Zhou, Y., Li, Z., Li, J., Zhao, R., Ding, X., 2018. Glacier mass balance in the Qinghai–Tibet Plateau and its surroundings from the mid-1970s to 2000 based on Hexagon KH-9 and SRTM DEMs. Remote Sens. Environ. 210, 96–112. https://doi.org/10.1016/j.rse.2018.03.020.
Zhu, M., Yao, T., Yang, W., Xu, B., Wu, G., Wang, X., Xie, Y., 2018. Reconstruction of the mass balance of Muztag Ata No. 15 glacier, eastern Pamir, and its climatic drivers. J. Glaciol. 64, 259–274. https://doi.org/10.1017/jog.2018.16.
Zhu, M., Yao, T., Xie, Y., Xu, B., Yang, W., Yang, S., 2020. Mass balance of Muji Glacier, northeastern Pamir, and its controlling climate factors. J. Hydrol. 590, 125447 https://doi.org/10.1016/j.jhydrol.2020.125447.
Zhu, M., Yang, W., Yao, T., Tian, L., Thompson, L.G., Zhao, H., 2021a. The influence of key climate variables on mass balance of Naimona'nyi glacier on a north-facing slope in the western Himalayas. J. Geophys. Res. Atmos. 126 https://doi.org/10.1029/2020JD033956 e2020JD033956.
Zhu, M., Thompson, L.G., Zhao, H., Yao, T., Yang, W., Jin, S., 2021b. Influence of atmospheric circulation on glacier mass balance in western Tibet: an analysis based on observations and modeling. J. Climate 34, 6743–6757. https://doi.org/10.1175/JCLI-D-20-0988.1.
Zhu, M., Yao, T., Thompson, L.G., Wang, S., Yang, W., Zhao, H., 2022a. What induces the spatiotemporal variability of glacier mass balance across the Qilian Mountains. Clim. Dynam. https://doi.org/10.1007/s00382-022-06283-4.
Zhu, M., Yao, T., Yang, W., Wu, G., Li, S., Zhao, H., Thompson, L.G., 2022b. Possible Causes of Anomalous Glacier Mass Balance in the Western Kunlun Mountains. J. Geophys. Res. Atmos. 127 (7) https://doi.org/10.1029/2021JD035705 e2021JD035705.